Applied Surface Science 518 (2020) 146236

Contents lists available at ScienceDirect

Applied Surface Science

journal homepage: www.elsevier.com/locate/apsusc

Full Length Article

Thickness dependent native oxidation kinetics observation and prediction for Cu films using spectroscopic ellipsometry

Jiamin Liu, Hao Jiang*, Lin Zhang, Honggang Gu, Xiuguo Chen, Shiyuan Liu*

State Key Laboratory for Digital Manufacturing Equipment and Technology, Huazhong University of Science and Technology, Wuhan 430074, China

ARTICLE INFO

Keywords:
Native oxidation
Thickness-dependency
Copper
Maxwell-Garnett EMA
Spectroscopic ellipsometry

ABSTRACT

Long-term native oxidation of polycrystalline Cu films with different thicknesses is investigated using spectroscopic ellipsometry. In order to more accurately determine the thickness of the oxide layer, a three-phase Maxwell-Garnett effective medium approximation model has been proposed to fit both the ellipsometric parameters and reflectance. X-ray photoelectron spectroscopy and transmission electron microscopy have been used to verify the rationality of the proposed model and measured results. The results demonstrate the Cabrera-Mott rule, and both the oxidation rate and the initial oxide thickness show significant dependencies on the thickness of Cu film. When thickness increases from 15 nm to 400 nm, the oxidation rate, defined as the slope in the inverse logarithmic correlation, decreases from 0.11/(nm·day) to 0.03/(nm·day) following an exponential function. Meanwhile, the initial oxide thickness, i.e. the intercept in the inverse logarithmic correlation, decreases from 0.73/nm to 0.3/nm in the light of a parabolic function. In the end, the oxidation evolution of a Cu film with arbitrary thickness is further predicted based on the obtained thickness-dependency, which is expected to provide a reference for better application of Cu films.

1. Introduction

Benefitting from the outstanding electric and thermal conductivities, electromigration resistance and mechanical properties, Cu is considered to be an excellent interconnect material in ultralarge-scale integration devices [1,2], a good conductive component in flexible circuits [3], and a metal-wire waveguide material in the terahertz system [4]. However, the native oxidation of Cu surface can degrade these physical properties, for instance that the native oxide on the Cu surface reduces the electric conductivity and the solderability [5], which consequently affects the widespread use of Cu in various field. Except for the above-mentioned adverse effects, the native oxides have compelling application value in other fields. The typical native cuprous oxide Cu_2O, which is a p-type semiconductor with a direct bandgap of 2.17 eV [6], has been widely used in the field of solar cells, thin film transistors and photo-catalysis [7–9]. While another native cupric oxide CuO, also as a p-type semiconductor with a narrow bandgap in the range of 1.21–1.51 eV [10], has been widely used as a supercapacitor material, magnetic storage media and gas sensing [11–13]. Practically, both Cu_2O and CuO are almost the most stable and typical oxide phases produced on the surface of Cu material during the native oxidation [6]. At this point, the native oxidation of Cu might be one of the potential ways to prepare the two semiconductor materials Cu_2O and CuO inexpensively [14]. Thus, it is of great importance to investigate the native oxidation dynamics of Cu films.

Up to now, various measurement methods, such as X-ray diffraction (XRD) [15], transmission electron microscopy (TEM) [16], X-ray photoelectron spectroscopy (XPS) [1,17,18] and spectroscopic ellipsometry (SE) [14,19,20], have been applied to the characterization of the short- or long-term native oxidation kinetics for Cu films. Specifically, Chu et al. revealed the crystalline structure property and the lattice parameters evolution of Cu_2O during the native oxidation of 23 h on the electropolished Cu(1 1 1) samples using XRD [15]. These results have been further applied to estimate the thickness of Cu_2O film in the initial stage of native oxidation. In the research work of Yang et al., transmission electron microscopy (TEM) measurements were used to determine the oxidation kinetics of single crystal Cu (0 0 1) within oxidation time of 1500 min in 760 Torr O_2 at 70 °C [16]. Although the oxidation kinetics obeys the Cabrera-Mott rule [21], the oxide layer gradually grows in the form of the nucleation and coalescence of oxide islands, which is different from the uniform growth fashion proposed by Cabrera and Mott [21]. However, due to the short period of the

* Corresponding authors at: School of Mechanical Science and Engineering, Huazhong University of Science and Technology, 1037 Luoyu Road, Wuhan, Hubei 430074, China (H. Jiang). State Key Laboratory for Digital Manufacturing Equipment and Technology, Huazhong University of Science and Technology, Wuhan 430074, China (S. Liu).

E-mail addresses: hjiang@hust.edu.cn (H. Jiang), shyliu@hust.edu.cn (S. Liu).

https://doi.org/10.1016/j.apsusc.2020.146236
Received 20 November 2019; Received in revised form 20 March 2020; Accepted 27 March 2020
Available online 27 March 2020
0169-4332/

observation, these trails failed to capture the formation of cupric oxide. Platzman et al. studied the relatively long-term oxide growth behavior on the surface of Cu film with thickness of 400 nm using XPS, as well as the thickness evolution of both Cu_2O and CuO phase [17]. The XPS results are instructive for understanding the three stages of native oxidation of bulk Cu. Further, SE has been introduced to investigate both the long-term native oxidation behaviors of Cu films with nominal thickness of 100 nm and bulk Cu by Lim et al [20]. The difference in the oxidation behavior has been analyzed and attributed to the difference in texture and microstructure between Cu films and bulk. However, neither the content evolution of CuO nor the quantitative difference in native oxidation behavior of Cu films and bulk have been systematically studied. Therefore, in order to ensure the better applications of nano-scale Cu films in the integrated circuits or the plasmon devices with the feature size shrinking, it is highly desirable to investigate the native oxidation behaviors of Cu films with different thicknesses.

Various kinetics laws including linear law, parabolic law, cubic law, logarithmic law and inverse-logarithmic law, have been introduced to describe the oxidation mechanism of Cu films and bulk [2,22–26]. These findings reveal the dependence of oxidation behavior of bulk Cu on temperature or pressure or types of crystallography. Moreover, it can be straightforward to infer from these results that the oxidation behavior of polycrystalline Cu film or bulk typically obeys the logarithmic law or the inverse-logarithmic law at the temperature below 150 °C and the pressure close to 101 kPa. However, the dependency of oxidation rate and initial oxide thickness on the thickness of Cu films are still unknown.

Compared to the methods such as XRD, TEM and XPS, SE is an effective approach to characterize the oxide thickness on Cu films in a non-destructive and high-precision manner. Especially for the study of long-term observation, SE ensures the rapid, successive and in-situ determination of the oxide thickness as a function of time. However, since the stratified model consisted of Cu_2O layer and Cu substrate was adopted in the previous research [17,19,26], ignoring the diversity in optical constants between Cu_2O and CuO and the non-layered growth characteristics of oxides, the deep understanding of the practical physical scenario such as the evolution of oxide components with oxidation time could not be provided. Diaz Leon *et al* used the three-phase Landau-Lifshitz-Looyenga (LLL) effective medium approximation (EMA) model to describe the effective dielectric functions of copper oxide film [14], which is motivated by the comparable thickness of oxide layer and the surface roughness. The LLL EMA model is more appropriate topologically for porous materials. Meanwhile, the LLL EMA model rarely considers the effects of Lorentz's local field correction, which is needed for the dielectric description of roughness layer. Through assuming an oxide layer and a roughness layer and consists of 50% material and 50% void, Platzman *et al* used the two-phase Bruggeman EMA model to describe the roughness layer on the oxide layer [17]. Meanwhile, the dielectric functions of oxide layer is described by a single-layer model consisted of CuO or Cu_2O, due to the similarity of the optical constants between the two oxide phases. Hu *et al* used an unclarified valid physical model to determine the thin oxide thickness from the spectroscopic reflectivity [19], and used the interference maxima formula to calculate the oxide thickness from the spectroscopic reflectivity. As for the refractive index of oxide phase, it was measured by spectroscopic ellipsometry. Although the method successfully characterizes the oxidation kinetics of Cu films under dry O_2, wet O_2 and steam, there possibly exists errors in the oxide thickness, which is caused by the significant uncertainty of interference peaks. O'Reilly used two optical models comprised of a Cu_2O layer on a Cu substrate and a Cu_2O on Cu on TiN to carry out the least squares fitting of ellipsometric parameters [26]. Correspondingly, the dynamic thicknesses of Cu_2O layer were extracted through the analysis. However, the effects of roughness layer on the Cu film were never considered. In fact, the coexistence of two oxide phases of Cu_2O and CuO in the native oxide layer of Cu film is widely studied and accepted [17,18,20]. Moreover, the surface roughness of Cu film leads to the inhomogeneous oxide growth on the Cu film, that is to say, the effects of the surface roughness layer and the oxide layer on the optical model are intertwined [17].

In this paper, the native oxidation kinetics of polycrystalline Cu films with different thicknesses has been investigated using SE over a long term, i.e. about 100 days, in order to extract the evolution of oxide layer thickness. Considering the significant dispersion of data in the three-phases LLL EMA analysis and the programming complexity in the three-phases Bruggeman EMA analysis, a stratified optical model based on three-phase Maxwell-Garnett EMA has been proposed for data analysis, which is demonstrated by the surface phase analysis reported by XPS results. Meanwhile, the accuracy of the oxide layer thickness determined by SE is confirmed by the oxygen and copper mappings, which is obtained by energy dispersive spectrometer (EDS) using the scanning transmission electron microscopy (STEM). Correspondingly, both the dynamic effective thicknesses of the oxides and the volume fractions of oxide component are calculated, and then the effective thicknesses have been analyzed based on the inverse-logarithmic rule to determine the oxidation rate and the initial oxide thickness. Further, the thickness dependencies of the oxidation rate and the initial oxide thickness are investigated based on two empirical functions. The former is described by an exponential function, while the latter is described by a parabolic function. With the achieved functions, the dynamic oxidation evolution on a Cu thin film with arbitrary thickness can be predicted.

2. Sample preparation and characterization methods

Copper films with different thicknesses were deposited on the pre-cleaned Si substrate covered with native oxide by magnetron dc-sputtering (TPR-450, China) [27]. The Cu target with purity of 99.999% was used in the deposition process. The base and work pressure were 5×10^{-3} Pa and 0.3 Pa, respectively. The sputtering temperature was 300 K and the sputtering atmosphere was Ar with purity of 99.99% in order to avoid the possible oxidation during the preparation. Since the sputtering power was set at a low value of 50 W, a rather low deposition rate of Cu film could be estimated as about 0.23 nm/sec. Through varing the deposition time, the Cu films with nominal thickness 15 nm, 23 nm, 32 nm, 60 nm, 100 nm and 400 nm were obtained. Immediately, the thickness of each Cu film was determined by measuring the height difference of lithography stairs using profilometer (Veeco NT-1100 PROFILER, Oxford Corporation, UK). The stairs were constructed using etching lithographically by etching away a part of the Cu film on the surface of Si substrate. And the detailed experimental procedures have been presented as Fig. 3 in Ref. [27]. As for the roughness metrology of each Cu film, it was observed by the white light interferometry (New-View 9000, Zygo Corporation Co., USA), in which the vertical and horizontal resolutions are 0.1 nm and 0.3 μm, respectively. Simultaneously, the dielectric functions of Cu films, covering the spectral range of 0.73–6.42 eV, were characterized by using spectroscopic ellipsometer (ME-L, Wuhan Eoptics Technology Co., Wuhan, China). Then, the Cu films were exposed to air at 300 K, 101 kPa and 50%RH, and therefore the native oxide would be gradually formed.

During the period of nearly 100 days, both ellipsometric parameters and reflectance were routinely measured by using the spectroscopic ellipsometer in the spectral range of 0.73–6.42 eV under the incident angle of 60°. The ellipsometric parameters were straightforwardly measured and reported by the ellipsometer, while the determination of reflectance needed two measurements consisted of a reference measurement and a sample measurement. The former was used to obtain the detected beam intensity reflected by a reference sample, which is a standard SiO_2 film on a Si substrate with the nominal thickness of 25 nm. While the latter was used to determine the intensity of reflected beam from each Cu film sample. By using the reflectance of the standard SiO_2 film sample from the library of the software for SE, the measured reflectance of each Cu film sample could be determined. The

corresponding detailed descriptions were also presented in Ref. [27]. It was worth noting that both the ellipsometric and reflectance measurements can be considered as a generalized in-situ condition because of two main reasons. At first, all the samples are stored in the same chamber with controlled temperature, pressure, oxygen content, as well as humidity. Second, since we selected the central area of the sample for observation, and the diameter of the detecting beam is about 5 mm, most of the area illuminated by the spot can be regarded as being overlapped at different trial. The oxidation phase of Cu films were investigated via the X-ray photoelectron spectrometer (XPS, VG Multilab 2000X) on the 7th day of oxidation. The morphology of Cu film was observed using a high-resolution transmission electron microscope (Tecnai F20, Thermo Fisher, USA), with the electron-transparent cross-section specimen prepared by using focused ion-beam bombardment (Helios 600i, Thermo Fisher, USA). Besides, the EDS mapping and the element line-scanning were obtained from the STEM (Talos F200X, Thermo Fisher, USA).

3. Theory for SE analysis

After the measurement of ellipsometric parameters and reflectance, a stratified optical model based on Fresnel optical interference is employed to fitting the measured results, thus the effective thickness and volume fraction of each oxide phase can be determined. The optical model consists of a Si substrate covered with native oxide layer, a Cu film followed by Cu oxide layer, and a layer of ambient air. Since the concentration of void in sputtered Cu film due to local internal stress is rather small [28], the dielectric response of Cu film can be described by a two-phase Maxwell-Garnett EMA with depolarization factor of 1/3 [29,30]. The corresponding expression is shown as Eq. (1),

$$\varepsilon_{eff} = \varepsilon_M \frac{(1 + 2f_{void})\varepsilon_{void} + (2 - 2f_{void})\varepsilon_M}{(1 - f_{void})\varepsilon_{void} + (2 + f_{void})\varepsilon_M}, \tag{1}$$

where ε_M and $\varepsilon_{void} = 1$ are the dielectric functions of Cu matrix and air void, respectively. ε_{eff} is the corresponding effective dielectric function. f_{void} is the volume fraction of void in the Cu film.

Since the effect of multi-constituents in the oxide layer and the effect of roughness are intertwined and indistinguishable [14], the three-phase Maxwell-Garnett EMA model with depolarization factor 1/3 has been proposed to describe the effective dielectric functions of the oxide layer. Similar to the two-phase Maxwell-Garnett or Bruggeman effective-medium models, the assuming that each inclusion phase is embedded in a homogenous medium with dielectric function ε_h is still valid in the native oxide layer. Correspondingly, the effective dielectric function ε_{oxide} of the native oxide layer can be expressed by the Clausius-Mossotti equation [31],

$$\varepsilon_{oxide} = \varepsilon_h \cdot [(1 + 2\langle\alpha\rangle)/(1 - \langle\alpha\rangle)], \tag{2}$$

where $< \alpha >$ represents the polarizability of the unit-cell volume in the native oxide layer. And the polarizability $< \alpha >$ is shown as Eq. (3),

$$\langle\alpha\rangle = f_1 \frac{\varepsilon_1 - \varepsilon_h}{\varepsilon_1 + 2\varepsilon_h} + f_2 \frac{\varepsilon_2 - \varepsilon_h}{\varepsilon_2 + 2\varepsilon_h} + f_3 \frac{\varepsilon_{void} - \varepsilon_h}{\varepsilon_{void} + 2\varepsilon_h}, \tag{3}$$

where ε_1 and ε_2 represent the dielectric functions of Cu_2O and CuO, respectively. f_1, f_2 and f_3 are the volume fractions of Cu_2O, CuO and the air void in the native oxide layer, respectively. Meanwhile, these volume fractions satisfy the law of summation, i.e. $f_1 + f_2 + f_3 = 1$. Combining Eqs. (2) and (3), the ε_{oxide} can be written as the following equation,

$$\varepsilon_{eff} = \varepsilon_h \cdot \left(1 + 2\sum_{i=1}^{2} \frac{\varepsilon_i - \varepsilon_h}{\varepsilon_i + 2\varepsilon_h} f_i + 2f_3 \frac{\varepsilon_{void} - \varepsilon_h}{\varepsilon_{void} + 2\varepsilon_h}\right) \Big/ \left(1 - \sum_{i=1}^{2} \frac{\varepsilon_i - \varepsilon_h}{\varepsilon_i + 2\varepsilon_h} f_i - f_3 \frac{\varepsilon_{void} - \varepsilon_h}{\varepsilon_{void} + 2\varepsilon_h}\right), \tag{4}$$

According to the results in Ref. [14], the volume fraction of Cu_2O is much larger than that of CuO before the oxidation of 70 days, while the volume fraction of CuO gradually becomes much larger after the roughly critical oxidation time. Correspondingly, the Cu_2O phase is selected as the host medium before the oxidation of 70 days, while CuO phase is selected as the host medium after the roughly critical oxidation time. Then, both the two cases satisfy the pre-requisite of applying the Maxwell-Garnett EMA model, which is that the volume fraction of the host medium is much larger than that of the inclusions [31]. Further, the effective dielectric functions of the native oxide layer can be expressed as Eqs. (5.a) and (5.b),

$$\varepsilon_{eff} = \varepsilon_1 \left[1 + 2f_2 \frac{\varepsilon_2 - \varepsilon_1}{\varepsilon_2 + 2\varepsilon_1} + 2f_3 \frac{\varepsilon_{void} - \varepsilon_1}{\varepsilon_{void} + 2\varepsilon_1}\right] \Big/ \left[1 - f_2 \frac{\varepsilon_2 - \varepsilon_1}{\varepsilon_2 + 2\varepsilon_1} - f_2 \frac{\varepsilon_{void} - \varepsilon_1}{\varepsilon_{void} + 2\varepsilon_1}\right], \tag{5.a}$$

$$\varepsilon_{eff} = \varepsilon_2 \left[1 + 2f_1 \frac{\varepsilon_1 - \varepsilon_2}{\varepsilon_1 + 2\varepsilon_2} + 2f_3 \frac{\varepsilon_{void} - \varepsilon_2}{\varepsilon_{void} + 2\varepsilon_2}\right] \Big/ \left[1 - f_1 \frac{\varepsilon_1 - \varepsilon_2}{\varepsilon_1 + 2\varepsilon_2} - f_3 \frac{\varepsilon_{void} - \varepsilon_2}{\varepsilon_{void} + 2\varepsilon_2}\right], \tag{5.b}$$

In the stratified optical model, the dielectric functions of Si substrate and native oxide layer are fixed as the results reported by Herzinger et al [32]. Meanwhile, the dielectric functions of Cu_2O and CuO are approximated as their corresponding bulk values [33], and their size-dependency has been omitted for simplification. Since the dielectric functions of metallic thin films are usually thickness-dependent as well, all the dielectric functions of Cu films are immediately measured by SE after sputtering and recorded as reference data for the oxide layer analysis in the next step [34,27]. The thickness of native SiO_2 layer on Si substrate has been determined previously by SE and the thickness of Cu film is fixed as the measurement values reported by the profilometer. Afterwards, the remaining parameters are chosen as the fitting parameters, which include the effective thickness of oxide layer d_{eff}, the volume fraction f_1 and f_2 of Cu_2O and CuO in the oxide layer, and the volume fraction f_{void} of void in the Cu film. All the fitting parameters will be determined by a spectral regressive analysis based on Levenberg-Marquardt algorithm [35–36], which is carried out via self-implemented program using MATLAB. The corresponding expression is shown as Eq. (6),

$$\chi^2 = \frac{1}{3N - M} \sum_{i=1}^{N} \left[\left(\frac{\psi_i^{meas} - \psi_i^{calc}}{\sigma(\psi_i^{meas})}\right)^2 + \left(\frac{\Delta_i^{meas} - \Delta_i^{calc}}{\sigma(\Delta_i^{meas})}\right)^2 + \left(\frac{R_i^{meas} - R_i^{calc}}{\sigma(R_i^{meas})}\right)^2\right], \tag{6}$$

where N and M are the number of wavelength points and fitting parameters, respectively. ψmeas i, Δmeas i and Rmeas i are the measured ellipsometric parameters and reflectance at the i^{th} wavelength, respectively. Meanwhile, ψcalc i, Δcalc i and Rcalc i refer to the calculated ellipsometric parameters and reflectance at the i^{th} wavelength, respectively. $\sigma(\psi$meas $i)$, $\sigma(\Delta$meas $i)$ and $\sigma(R$meas $i)$ stand for the estimated standard deviation of ψmeas i, Δmeas i and Rmeas i. χ^2 represents the root mean square error.

4. Results and discussions

Table 1 shows the measured thickness of each Cu film reported by profilometer. Meanwhile, the roughness reported by white light interferometry is also presented in Table 1. Without losing generality, we compared the thickness measurement on the sample with nominal thickness of 23 nm with the result reported by TEM, which is 22.1 nm. The method for the Cu film thickness measurement has been proposed and demonstrated in the literature [27]. These results ensure the

Table 1
The sputtering time and thickness of Cu films.

Sputtering time [sec]	Nominal thickness [nm]	Measured thickness [nm]	Roughness [nm]
50	15	14.5 ± 0.46	1.5 ± 0.04
95	23	24.2 ± 0.62	2.2 ± 0.07
140	32	27.4 ± 0.36	2.3 ± 0.10
260	60	58.5 ± 1.60	1.7 ± 0.11
450	100	99.3 ± 2.01	1.2 ± 0.35
2700	400	426.2 ± 3.87	2.5 ± 0.51

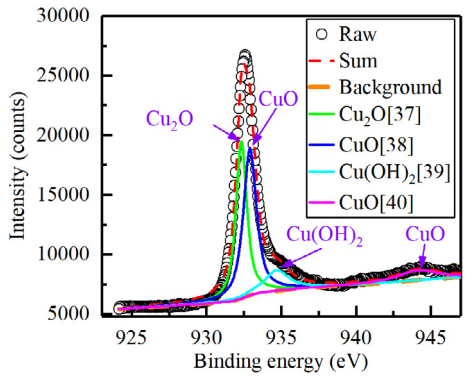

Fig. 1. XPS spectra of Cu film with nominal thickness of 15 nm on the 7th days of native oxidation.

reliability of the thickness of Cu film reported by the profilometer.

4.1. XPS spectra

After native oxidation of 7 days, an XPS study of the Cu film with nominal thickness of 15 nm was carried out to determine the surface oxide phase and the results are shown in Fig. 1. For simplicity and briefness, not all the XPS results are shown here, since the results of other Cu films are highly similar to the one shown in Fig. 1. The Cu $2p_{3/2}$ spectra exhibit four peaks, which correspond to Cu_2O peak at 932.3 eV [37], CuO peak at 932.9 eV [38], $Cu(OH)_2$ peak at 934.7 eV [39] and CuO satellite peak at 944.8 eV [40], respectively. Since the $Cu(OH)_2$ phase is metastable and can easily transform into the CuO phase [17], the influence of $Cu(OH)_2$ phase on the effective dielectric functions of oxide layer can be omitted. Further, owing to the fast transformation of $Cu(OH)_2$ phase to CuO phase in the studied aqueous ambient [17], once the $Cu(OH)_2$ is formed through the interaction between the Cu ions and hydroxyl groups, the cupric oxide will be produced immediately. Accordingly, the presence of $Cu(OH)_2$ phase in the XPS spectra indicates that the formation of CuO phase is a continuing oxidation process. The coexistence of Cu_2O phase and CuO in the XPS spectra reflects the oxide layer consists of Cu_2O phase and CuO phase, which verifies the rationality of the three phase Maxwell-Garnett EMA model. Notably, the peak intensities of the Cu_2O phase at 932.3 eV and the CuO phase at 932.9 eV are comparable, indicating that the formation of CuO phase is much earlier than the possible critical time of 320 h for CuO layer formed on Cu film prepared by ion beam deposition [18].

4.2. SE and analysis

During the oxidation, both the ellipsometric parameters and reflectance of each Cu film have been measured by using the spectroscopic ellipsometer. Correspondingly, the dynamic ellipsometric parameters and reflectance of Cu film with nominal thickness of 32 nm are presented in Fig. 2. It can be observed that, with the oxidation time increasing, the amplitude-ratio angle ψ is shifted upward as a whole, while both the phase difference Δ and the reflectance exhibit overall downward trends.

As for the Cu films with other thicknesses, since the overall evolution trends of ψ, Δ and reflectance with oxidation time are similar to the results shown in Fig. 2, only the evolution trends of both ψ, Δ and reflectance at 2.17 eV with oxidation time would be presented in the figure. The corresponding results are shown in Fig. 3. The amplitude-ratio angle ψ of all the Cu films shows a slight increasing trend with the oxidation time increasing, and the phase difference Δ exhibits a slight decreasing trend, while the reflectance shows the insufficiently obvious changing trend. Moreover, it can be observed that the ψ, Δ and reflectance curves with different thicknesses are almost parallel to each other, which indicates similar growth behavior of oxides on the film surface, and then resulting in similar changes of ψ, Δ and reflectance. Besides, it can be noticed that there exists a significant decrease of the reflectance from about 65% to 20% observed for the 400 nm-thick Cu film after the oxidation of 103 days, which might be caused by an unexpected performance instability issue of the instrument during the reflectance measurement. When we check the parallel data collected with the incident angle of 70°, the corresponding measured reflectance looks normal. Although the local measurement error shown in Fig. 3(c) is awful, it does not obviously affect the thickness determination in the fitting analysis. Considering the reflectance is mainly related to the refractive index of native oxide, the dominate constraint from the reflectance on the fitting analysis is the line-shape of the reflectance curve. Since the dielectric functions of Cu_2O, CuO and the air void in the oxide layer are fixed as the given values, the whole changes of dielectric functions of the oxide layer can only be adapted by the volume fractions. Correspondingly, the line-shape of the reflectance has a more significant effect on the decoupling the effective thickness and the volume fraction than the local value of reflectance. In addition, we carried out a set of parametric analysis to evaluate the effects of measurement error of the reflectance in the next paragraph.

Further, the synergic regression analysis of measured ψ, Δ and reflectance has been carried out to determine the effective thickness d_{eff} of oxide layer and the volume fraction of each component in the oxide layer. Through adapting the oxide thickness d_{eff}, the volume fraction f_1 and f_2 of Cu_2O and CuO in the oxide layer, and the volume fraction f_{void} of void in the Cu film, the calculated ellipsometric parameters and reflectance would be computed by the stratified optical model and be fitted to the measured ones. With the minimum value of root mean square error for the fitting analysis being obtained, the corresponding oxide thickness and the volume fractions of oxide phases would be determined. Without loss of generality, the fitting results of Cu film with nominal thickness of 32 nm after oxidation of 30 days are shown in Fig. 4 to show the goodness of the fitting. The results in Fig. 4 show that the measured ψ, Δ and reflectance are well fitted overall with the values calculated using the stratified optical model. In order to quantify the effects of measurement error of the reflectance on the native oxide layer thickness determination of the 400 nm Cu film after oxidation of 103 days, we carried out a set of parametric analysis. With all the procedure and parameters fixed, we used the reflectance achieved at incident angle of 60° and 70°, and respectively achieve the oxide thicknesses of 6.24 nm and 6.02 nm. As an additional comparison, we carried out a fitting analysis using the ellipsometric parameters only, and the corresponding oxide layer thickness is 6.14 nm. The consistency among the three values indicates that the effect on the inverse solution of local reflectance value might be significantly weaker than that of the reflectance curvature shape. It is worth to comment here that the fitting results of measured ψ, Δ and reflectance of the films with other thicknesses are similar to those shown in Fig. 4. It is worth to note that there is a fitting deviation in the spectral range of the photon energy above 4.7 eV, which can be attributed to the insufficiently accurate dielectric functions of Cu_2O and CuO taken from literature [33]. In order to accurately correlate the effective dielectric functions of the oxide layer to the volume fractions, both the dielectric functions of Cu_2O and CuO are

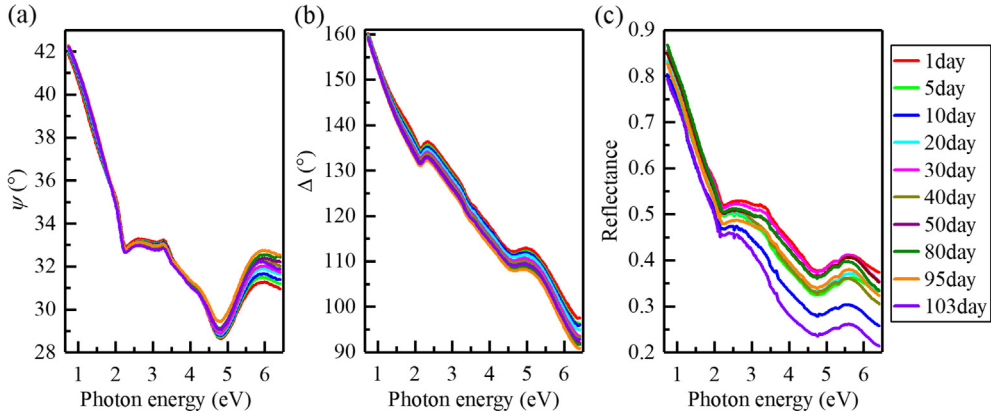

Fig. 2. The dynamic ellipsometric parameters and reflectance of Cu film with nominal thickness of 32 nm over a period of nearly 100 days. (a) The amplitude-ratio angle ψ, (b) the phase difference Δ, and (c) the reflectance.

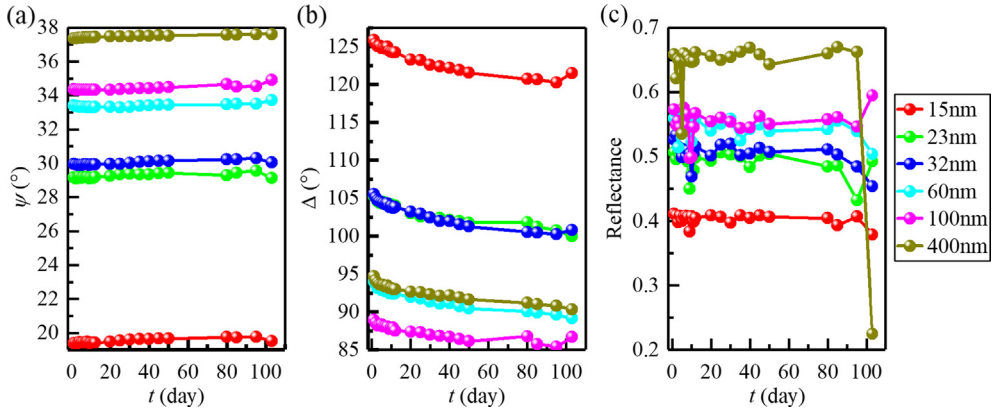

Fig. 3. The dynamic ellipsometric parameters and reflectance of each Cu film at 2.17 eV over a period of nearly 100 days. (a) The amplitude-ratio angle ψ, (b) the phase difference Δ, and (c) the reflectance.

fixed as the given values. The measurement of the dielectric functions in the high photon-energy range is much more difficult than that in the range from the near infrared to visible light, and the sample dependency may become significant. Therefore, the corresponding consistency may be lower. Considering the data points below 4.7 eV dominate the fitting results, it is rational to observe a fitting deviation above 4.7 eV. However, the line-shapes of ellipsometric parameters and reflectance dominate the thickness determination rather than the local values of the ellipsometric parameters and reflectance do. Thus, although the fitting deviation above 4.7 eV exists, the thickness fittings are still reliable according to the good fitting of line-shapes of Ψ and R, and the good fitting of Δ.

Meanwhile, the effective thickness d_{eff} of each oxide layer on the surface of corresponding Cu film over a period of nearly 100 days has been calculated. Considering that the native oxidation of Cu films at room temperature obeys the Cabrera-Mott rule [21], the inverse-logarithmic analysis has been carried out for the effective thickness d_{eff}, shown as Eq. (7).

$$\frac{1}{d_{eff}} = A - B\ln t, \tag{7}$$

where A and B are the intercept and the slope factor in the inverse-logarithmic law, respectively. t is the oxidation time, whose unit is day.

The analysis results are shown in Fig. 5(a). According to the results

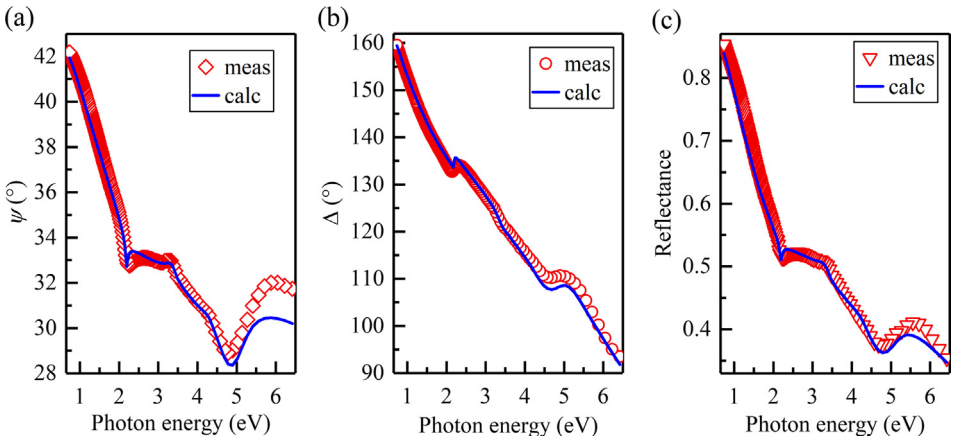

Fig. 4. The fitting results of ellipsometric parameters and reflectance of Cu film with nominal thickness of 32 nm after oxidation of 30 days. (a) The fitting result of amplitude-ratio angle ψ, (b) the fitting result of phase difference Δ, and (c) the fitting result of reflectance. Open symbols represent the measurement values in (a), (b) and (c), respectively, while solid lines stand for the calculated values.

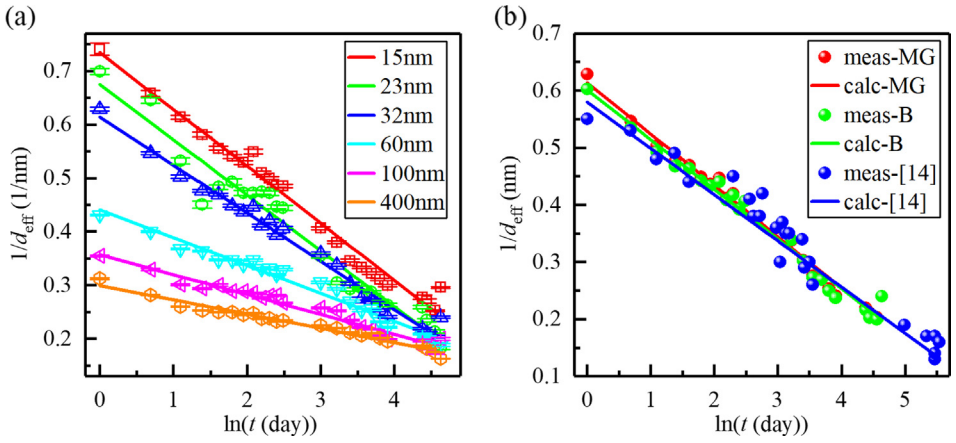

Fig. 5. The results of inverse-logarithmic analysis for the oxide thickness. (a) The inverse thickness of oxide and its error bars for all the Cu films, (b) the comparison between the inverse thicknesses in our work and in the literature [14]. In both 5(a) and 5(b), dot stands for the measured values, and line presents the fitting results calculated from Eq. (7).

in Fig. 5(a), all the measured oxide thickness, stood by dots, can be well fitted with the calculated values obtained by Eq. (7). Moreover, as the nominal thickness of Cu film increases from 15 nm to 400 nm, both the slope and the intercept decrease, which clearly exhibits the film thickness dependency. As the oxidation time increases, all the oxide thicknesses exhibit an increasing trend, i.e. the inverse thickness decreasing. Moreover, the oxide growth in the early oxidation stage of less than 10 days is faster, while the subsequent growth becomes slightly slower as shown by the increasing density of the data points. Besides, with the multiple repeated measurements, the error bars from the standard deviation of each inverse thickness of oxide layer are alos estimated and shown in Fig. 5(a). It can be noticed that all the error bars are very small, indicating that the variations of measurement results from one sample to another sample are quite small and ignorable.

For demonstration, the inverse thickness of the oxide layer on the Cu film with nominal thickness of 32 nm has been compared to the results from both three-phase Bruggeman EMA analysis and three-phase LLL EMA analysis [14], and the good agreements are achieved as shown in Fig. 5(b). The slope and intercept from the three-phase Maxwell-Garnett EMA analysis in our experiment are 0.0898/(nm·day) and 0.614/nm, respectively, while the corresponding values from the three-phase Bruggeman EMA analysis in our experiment are 0.0869/(nm·day) and 0.601/nm, respectively. Moreover, the reported values from the three-phase LLL EMA analysis in literature [14] are 0.08/(nm·day) and 0.58/nm, respectively. The nearly consistent slope and intercept indicate the similar accuracy. As for the little discrepancies, there are two possible reasons for it: (1) the different thickness of Cu film caused by different sputtering parameters, (2) the different EMA model of oxide. The measured thickness of Cu film in our work is 27.41 nm, while the measured values in the literature [14] is 32 nm. Therefore, it is rational that the slope factor in our work is slightly larger than the literature value.

In order to further demonstrate the accuracy of the measured thickness of oxide, TEM sectional observation, elements line-distribution, copper and oxygen mappings were also performed and the results are shown in Fig. 6. The oxide thickness in the sectional view shown in Fig. 6(a) is 3.3 nm, which corresponds to the oxide thickness on the Cu film with nominal thickness of 32 nm after oxidation of 25 days. In contrast, the measured thickness of the oxide layer on the parallel sample reported by SE is 2.95 nm. Meanwhile, the sectional view also exhibits that the oxide film on the surface of Cu film is discontinuous. This discontinuity not only shows the localized characteristics of oxide formation, but also indicates the high uncertainty of thickness measured by TEM. Fig. 6(b) shows the elements line-distribution of Cu film with nominal thickness of 400 nm after oxidation of 100 days, which is reported by the STEM. According to Fig. 6(b), the Cu- and O-rich region corresponds to the native oxide layer, and the region width of nearly 5.5 nm indicates the possible thickness of the oxide layer. Further, the Cu- and O-mappings were also been obtained by EDS using scanning TEM, as shown in Fig. 6(c) and (d), respectively. The overlapping region between Cu- and O- mappings represents the native oxide layer, and the thickness is estimated as about 5.5 nm, while the measured thickness given by SE is 5.71 nm. Besides, it can be noticed that the layer of oxygen mapping is laterally fluctuating in Fig. 6(d), which reveals the thickness inhomogeneity of oxides caused by the original surface morphology of Cu film. In other words, both the oxide layer and the surface roughness layer on the Cu films are intertwining, which once again proves the rationality of three-phase EMA model.

Accompanying with the determination of the effective thickness of native oxide layer, the volume fraction f_{void} of air void in the Cu film layer, the volume fractions f_1 and f_2 of Cu_2O and CuO in the oxide layer are also obtained from the fitting analysis. The volume fraction f_{void} is less than 1% and no noticeable changes have been observed during the oxidation process, which indicates no obvious correlation between the volume fraction of air void in the Cu film layer and the oxidation dynamics on the surface of Cu films. As for the dynamic volume fractions f_1 and f_2 of Cu_2O and CuO, the former decreases with the oxidation time increasing, while the latter increases, and followed by a trend of convergence, as shown in Fig. 7. The results indicate the transformation of Cu_2O phase to CuO phase. Moreover, the total volume fraction of Cu_2O and CuO is much less than 100%, which ensures the physical rationality. Although the uncertainties of the achieved dynamic volume fractions are relatively large, they won't affect the accuracy of the effective thickness determination.

4.3. Thickness-dependency of oxide

Through the above inverse-logarithmic analysis, the slopes and the intercepts corresponding to the Cu films with different thicknesses have been determined. Further, the thickness dependency of the slope is further analyzed and fitted by an exponential function, and the thickness dependency of the intercept has been fitted by a parabolic function. Correspondingly, the fitting results are shown in Fig. 8(a) and (b), respectively. As the logarithmic thickness of Cu film increases from 2.674 nm to 6.055 nm, the slope factor decreases from 0.106/(nm·day) to 0.027/(nm·day), and the intercept decreases from 0.734/nm to 0.299/nm. Meanwhile, the empirical formula obtained from the fitting procedures are shown as Eq. (8),

$$B = 0.421 \cdot \exp[-0.485 \cdot ln(d_{Cu})], \tag{8a}$$

$$A = 0.043 \cdot [ln(d_{Cu}) - 6.001]^2 + 0.292, \tag{8b}$$

where B and A are the slope factor and intercept, respectively. d_{Cu} is the effective thickness of Cu film.

Notably, the mean square error (MSE) of 4.278×10^{-4} and the coefficient of determination of 0.9301 in Fig. 8(a) indicate the fitting results are acceptable. And the MSE and the coefficient of

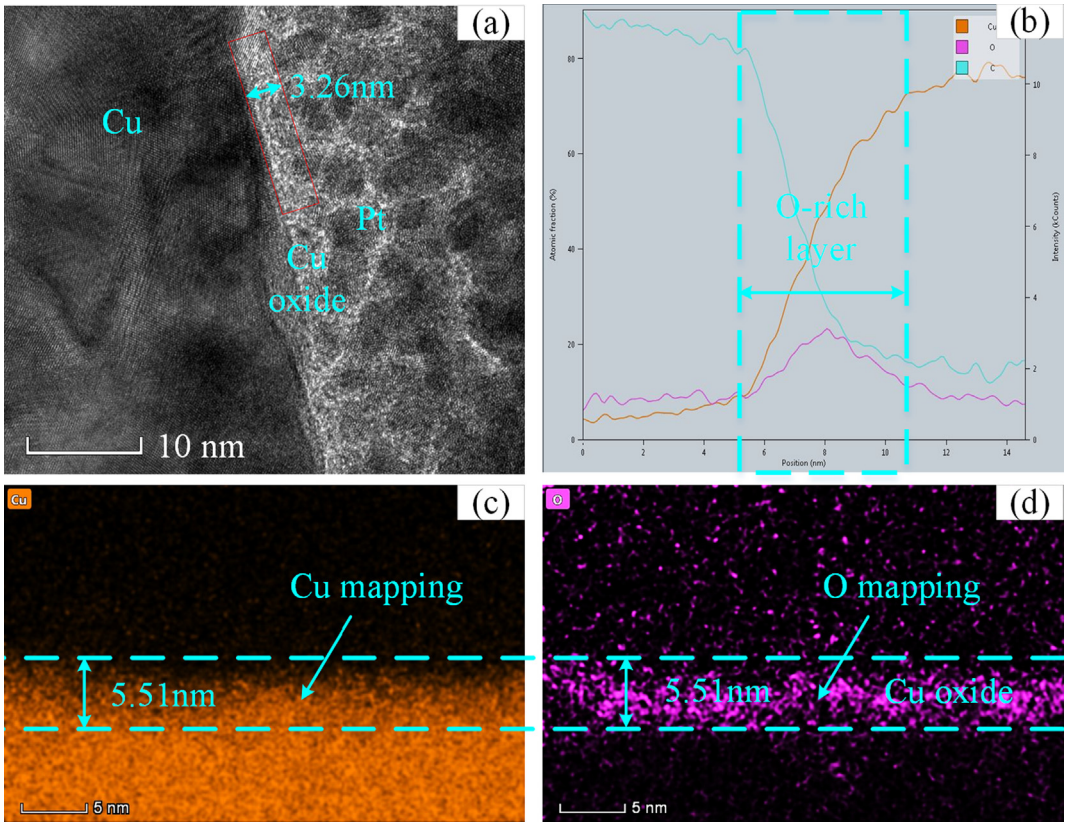

Fig. 6. The observed results of Cu film with nominal thickness of 32 nm and 400 nm by TEM, line-scanning and EDS mapping. (a) The TEM sectional view of Cu film with nominal thickness of 32 nm after oxidation of 25 days, (b) the elements line-distribution of Cu film with nominal thickness of 400 nm after oxidation of 100 days, (c) and (d) copper and oxygen mappings of Cu film with nominal thickness of 400 nm after oxidation of 100 days,

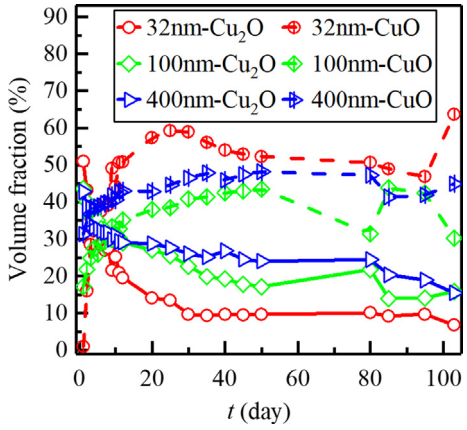

Fig. 7. The time-dependent volume fractions of Cu_2O and CuO on the surface of Cu films with nominal thicknesses of 32 nm, 100 nm and 400 nm.

determination for the intercept approximation are 0.0036 and 0.9773, respectively. Since the slope is a measure of the inverse growth rate of the oxide layer, and the intercept is a measure of the initial inverse thickness of the oxide layer, the thickness-dependencies shown in Fig. 8(a) and (b) reveal that both the growth rate and the initial thickness of oxide are dependent on the thickness of Cu film. With the film thickness increasing, both the growth rate and the initial thickness of oxide increase. This phenomenon can be interpreted based on the Cabrera-Mott theory. Usually, the onset of native oxidation is started by the dissociative adsorption of O_2 [17], in which a strong electric field has been set up due to the contact potential difference between adsorbed oxygen and metal [21]. The formation of Cu_2O is driven by the electric field. Since the concentration of the positive ions of Cu at the Cu film/oxide interface increases with the thickness of Cu film increasing, both the concentration of adsorbed O_2 and field strength also increases with respect to the thickness of Cu film. Therefore, the initial thickness of oxide on a thicker Cu film is larger than that on a thinner Cu film. Simultaneously, the migration of Cu cations is more intense on the surface of the thicker Cu film due to the formed electric field.

Further, based on Eqs. (7) and (8), it is possible to predict the oxide thickness of the Cu film with an arbitrary thickness after a certain oxidation time. The predicted results are shown in Fig. 9. As shown in Fig. 9, the thickness of Cu film ranges from 5 nm to 400 nm, and the oxidation time ranges from 1 day to 100 days. The thickness of oxide on the surface of Cu film is estimated as a value ranging from 0.88 nm to 6.12 nm. These results will be used as a reference in the applications of Cu and as a guidance in the preparation of Cu oxide.

5. Conclusions

In summary, the growth process of native oxide on the surface of polycrystalline Cu films with different thicknesses during a long period of nearly 100 days has been investigated using spectroscopic ellipsometry. The thickness dependencies of both growth rate and initial thickness of oxide have been revealed based on a stratified optical model based on three-phase Maxwell-Garnett EMA and the inverse-logarithmic analysis. In the proposed model, the oxide is always assumed to consist of Cu_2O, CuO and void. In order to determine the oxide thickness, the ellipsometric parameters and reflectance reported by ellipsometer have been fitted with the values calculated by the optical model. Surface phase analysis reported by XPS is used to validate the rationality of the EMA model, and the oxide thickness and oxygen mapping obtained by TEM are used to confirm the accuracy of oxide thickness. Further, the thickness dependency of growth rate and initial oxide thickness of oxide has been observed and quantified via an

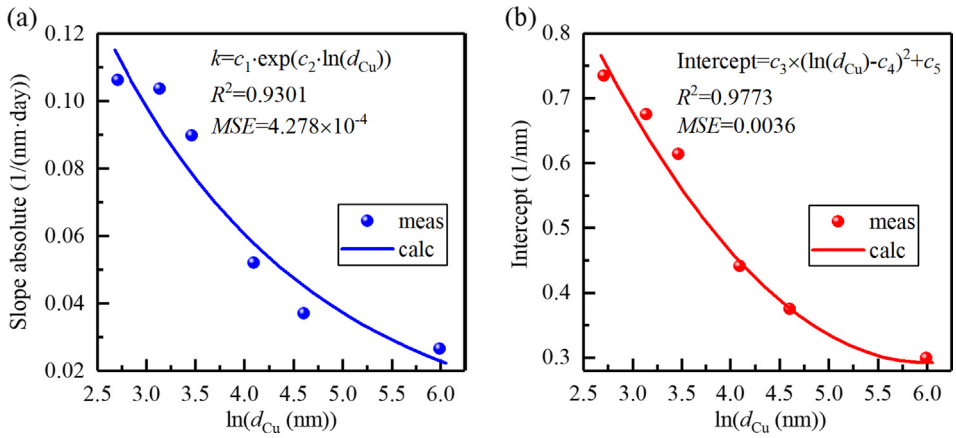

Fig. 8. The fitting results of slope factor and intercept. (a) The fitting results for the thickness-dependency of the slope factor on the thickness of Cu film, (b) the fitting results for the thickness-dependency of the intercept on the thickness of Cu film.

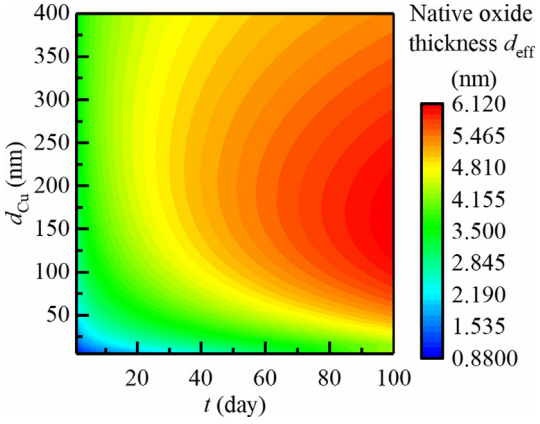

Fig. 9. The native oxide thickness evolution predicted for a Cu film with arbitrary thickness. The thickness of Cu film ranges from 5 nm to 400 nm, and the oxidation time ranges from 1 day to 100 days.

inverse logarithmic analysis. With the film thickness increasing from 14.5 nm to 426.2 nm, the oxidation rate, namely the slope in the inverse logarithmic law, decreases from 0.11/(nm·day) to 0.03/(nm·day) according to an exponential function. The initial oxide thickness, namely the intercept in the inverse logarithmic law, decreases from 0.73/nm to 0.3/nm in the light of the parabolic function. With the achieved thickness-dependency correlation, the oxide layer evolution on a Cu thin film with an arbitrary thickness can be predicted.

CRediT authorship contribution statement

Jiamin Liu: Conceptualization, Methodology, Formal analysis, Investigation, Software, Writing - original draft. **Hao Jiang:** Conceptualization, Methodology, Investigation, Validation, Writing - review & editing, Supervision, Project administration, Funding acquisition. **Lin Zhang:** Investigation, Resources. **Honggang Gu:** Writing - review & editing. **Xiuguo Chen:** Writing - review & editing. **Shiyuan Liu:** Writing - review & editing, Project administration, Funding acquisition.

Declaration of Competing Interest

The authors declare that they have no known competing financial interests or personal relationships that could have appeared to influence the work reported in this paper.

Acknowledgements

This work was funded by the National Natural Science Foundation of China (Grant No. 51525502, 51975232, 51575214, and 51727809); the National Key Research and Development Plan (Grant No. 2017YFF0204705); the Natural Science Foundation of Hubei Province of China (Grant No. 2018CFA057); and the National Science and Technology Major Project of China (Grant No. 2017ZX02101006-004). We would like to thank Ms. Yan Zhu and Mr. Jianlin Chu for FIB processing and White Light Interferometer measurement in Micro and Nano Fabrication and Measurement Laboratory of Collaborative Innovation Center for Digital Intelligent Manufacturing Technology and Application.

References

[1] P. Keil, R. Frahm, D. Lutzenkirchen-Hecht, Native oxidation of sputter deposited polycrystalline copper thin films during short and long exposure times: comparative investigation by specular and non-specular grazing incidence X-ray absorption spectroscopy, Corros. Sci. 52 (2010) 1305–1316.
[2] K. Fujita, D. Ando, M. Uchikoshi, K. Mimura, M. Isshiki, New model for low-temperature oxidation of copper single crystal, Appl. Surf. Sci. 276 (2013) 347–358.
[3] G.K.P. Ramanandan, G. Ramakrishnan, P.C.M. Planken, Oxidation kinetics of nanoscale copper films studied by terahertz transmission spectroscopy, J. Appl. Phys. 111 (2012) 123517.
[4] T. Jeon, J. Zhang, D. Grischkowsky, THz Sommerfeld wave propagation on a single metal wire, Appl. Phys. Lett. 86 (2005) 161904.
[5] M. Ramirez, L. Henneken, S. Virtanen, Oxidation kinetics of thin copper films and wetting behaviour of copper and organic solderability preservatives (OSP) with lead-free solder, Appl. Surf. Sci. 257 (2011) 6481–6488.
[6] C. Gattinoni, A. Michaelides, Atomistic details of oxide surfaces and surface oxidation: the example of copper and its oxides, Surf. Sci. Rep. 70 (2015) 424–447.
[7] K.P. Musselman, A. Wisnet, D.C. Iza, H.C. Hesse, C. Scheu, J.L. MacManus-Driscoll, L. Schmidt- Mende, Strong efficiency improvements in ultra-low-cost inorganic nanowire solar cells, Adv. Mater. 22 (2010) E254–E258.
[8] E. Fortunato, V. Figueiredo, P. Barquinha, E. Elamurugu, R. Barros, G. Goncalves, S.K. Park, C. Hwang, R. Martins, Thin-film transistors based on p-type Cu_2O thin films produced at room temperature, Appl. Phys. Lett. 79 (2010) 192102.
[9] A. Soon, X. Cui, B. Delley, S. Wei, C. Stampfl, Native defect-induced multifarious magnetism in nonstoichiometric cuprous oxide: first-principles study of bulk and surface properties of $Cu_{2-\delta}O$, Phys. Rev. B 79 (2009) 035205.
[10] L. De Los Santos, D. Hurtado Valladares, A. Bustamante Salinas, D. Acosta Dominguez, S.I. Najarro, T. Khondaker, C.H.W. Mitrelias, J. Albino Barnes, Y. Majima Aguiar, Crystallization and electrical resistivity of Cu_2O and CuO obtained by thermal oxidation of Cu thin films on SiO_2/Si substrates, Thin Solid Films 520 (2012) 6368–6374.
[11] A.S. Zoolfakar, R.A. Rani, A.J. Morfa, A.P. O'Mullane, K. Kalantar-zadeh, Nanostructured copper oxide semiconductors: a perspective on materials, synthesis methods and applications, J. Mater. Chem. C 2 (2014) 5247–5270.
[12] R.A. Borzi, S.J. Stewart, R.C. Mercader, G. Punte, F. Garcia, Magnetic behavior of nanosized cupric oxide, J. Magn. Magn. Mater. 226–230 (2001) 1513–1515.
[13] C. Yang, X. Su, F. Xiao, J. Jian, J. Wang, Gas-sensing properties of CuO nanorods synthesized by a microwave-assisted hydrothermal method, Sensor. Actuat. B-Chem. 158 (2011) 299–303.
[14] J.J. Diaz Leon, D.M. Fryauf, R.D. Cormia, M.X.M. Zhang, K. Samuels, R. Stanley Williams, N.P. Kobayashi, Reflectometry-ellipsometry reveals thickness, growth

rate, and phase composition in oxidation of copper, ACS Appl. Mater. Interfaces 8 (2016) 22337–22344.
[15] Y.S. Chu, I.K. Robinson, A.A. Gewirth, Comparison of aqueous and native oxide formation on Cu(111), J. Chem. Phys. 110 (1999) 5952–5959.
[16] J.C. Yang, B. Kolasa, J.M. Gibson, M. Yeadon, Self-limiting oxidation of copper, Appl. Phys. Lett. 73 (1998) 2841–2843.
[17] I. Platzman, R. Brener, H. Haick, R. Tannenbaum, Oxidation of polycrystalline copper thin films at ambient condition, J. Phys. Chem. C 112 (2008) 1101–1108.
[18] J. Iijima, J.-W. Lim, S.-H. Hong, S. Suzuki, K. Mimura, M. Isshiki, Native oxidation of ultra high purity Cu bulk and thin films, Appl. Surf. Sci. 253 (2006) 2825–2829.
[19] Y.Z. Hu, R. Sharangpani, S.-P. Tay, Kinetic investigation of copper film oxidation by spectroscopic ellipsometry and reflectometry, J. Vac. Sci. Technol. A 18 (2000) 2527–2532.
[20] J.-W. Lim, J. Iijima, Y. Zhu, J.H. Yoo, G.-S. Choi, K. Mimura, M. Isshiki, Nanoscale investigation of long-term native oxidation of Cu films, Thin Solid Films 516 (2008) 4040–4046.
[21] N. Cabrera, N.F. Mott, Theory of the oxidation of metals, Rep. Prog. Phys. 12 (1949) 163–184.
[22] M. Rauh, P. Wißmann, The oxidation kinetics of thin copper films studied by ellipsometry, Thin Solid Films 228 (1993) 121–124.
[23] B. Maack, N. Nilius, In-situ optical view onto copper oxidation - role of reactive interfaces and self-heating, Corros. Sci. 159 (2019) 108112.
[24] F.W. Young Jr., J.V. Cathcart, A.T. Gwathmey, The rates of oxidation of several faces of a single crystal of copper as determined with elliptically polarized light, Acta Metallurgica 4 (1956) 145–152.
[25] S.K. Roy, S.C. Sircar, A critical appraisal of the logarithmic rate law in thin-film formation during oxidation of copper and its alloys, Oxid. Met. 15 (1981) 9–20.
[26] M. O'Reilly, X. Jiang, J.T. Beechinor, S. Lynch, C. Ni Dheasuna, J.C. Patterson, G.M. Crean, Investigation of the oxidation behaviour of thin film and bulk copper, Appl. Surf. Sci. 91 (1995) 152–156.
[27] J. Liu, J. Lin, H. Jiang, H. Gu, X. Chen, C. Zhang, G. Liao, S. Liu, Characterization of dielectric function for metallic thin films based on ellipsometric parameters and reflectivity, Phys. Scr. 94 (2019) 085802.
[28] D.E. Aspnes, E. Kinsbron, D.D. Bacon, Optical properties of Au: sample effects, Phys. Rev. B 21 (1980) 3290–3299.
[29] R.W. Cohen, G.D. Cody, M.D. Coutts, B. Abeles, Optical properties of granular silver and gold films, Phys. Rev. B 8 (1973) 3689–3703.
[30] J.E. Spanier, I.P. Herman, Use of hybrid phenomenological and statistical effective-medium theories of dielectric functions to model the infrared reflectance of porous SiC films, Phys. Rev. B 61 (2000) 10437–10450.
[31] V.A. Markel, Introduction to the Maxwell Garnett approximation: tutorial, J. Opt. Soc. Am. A 33 (2016) 1244–1256.
[32] C.M. Herzinger, B. Johs, W.A. McGahan, J.A. Woollam, W. Paulson, Ellipsometric determination of optical constants for silicon and thermally grown silicon dioxide via a multi-sample, multi-wavelength, multi-angle investigation, J. Appl. Phys. 83 (1998) 3323–3336.
[33] E.D. Palik, Handbook of Optical Constants of Solid, Academic Press, San Diego, 1998.
[34] H. Fujiwara, Spectroscopic Ellipsometry Principles and Application, John Wiley & Sons Ltd, Chichester, 2007.
[35] K. Levenberg, A method for the solution of certain nonlinear problems in least squares, Quart. Appl. Math. 2 (1944) 164–168.
[36] D.W. Marquardt, An algorithm for least squares estimation of non-linear parameters, J. Soc. Indust. Appl. Math. 11 (1963) 431–441.
[37] G. Ertl, R. Hierl, H. Knözinger, N. Thiele, H.P. Urbach, XPS study of copper aluminate catalysts, Appl. Surf. Sci. 5 (1980) 49–64.
[38] Z. Hussain, M.A. Salim, M.A. Khan, E.E. Khawaja, X-ray photoelectron and auger spectroscopy study of copper-sodium-germanate glasses, J. Non-Cryst. Solids 110 (1989) 44–52.
[39] G. Deroubaix, P. Marcus, X-ray photoelectron spectroscopy analysis of copper and zinc oxides and sulphides, Surf. Interface Anal. 18 (1992) 39–46.
[40] F. Parmigiani, G. Pacchioni, F. Illas, P.S. Bagus, Studies of the Cu-O bond in cupric oxide by X-ray photoelectron spectroscopy and ab initio electronic structure models, J. Electron Spectrosc. Relat. Phenom. 59 (1992) 255–269.